Journal of Materials Chemistry A

Accepted Manuscript

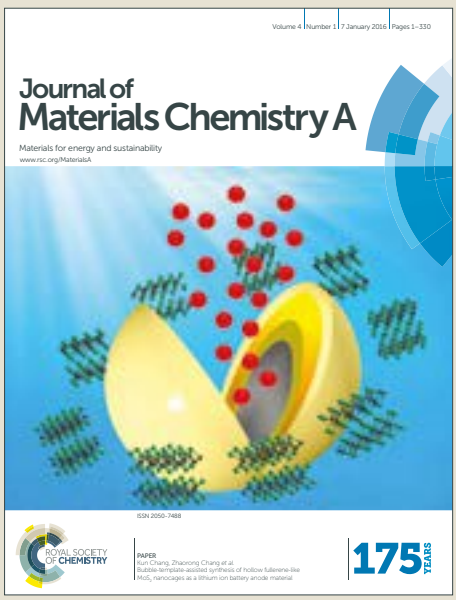

ROYAL SOCIETY OF CHEMISTRY

rsc.li/materials-a

View Article Online
DOI: 10.1039/C8TA11812D

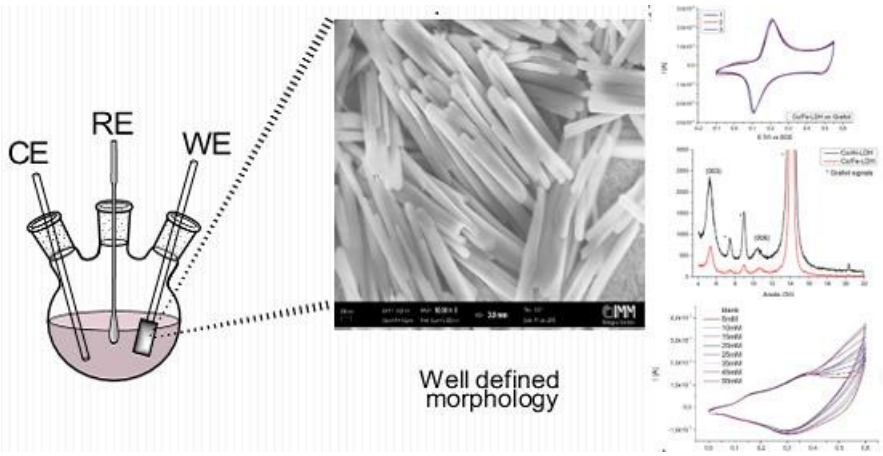

Novel and reproducible protocol allows the electro-synthesis of LDHs for electro-catalytic application.

View Article Online
DOI: 10.1039/C8TA11812D

Journal Name

ARTICLE

Newly developed electrochemical synthesis of Co-based Layered Double Hydroxides: toward noble metal-free electro-catalysis

Elisa Musella[a], Isacco Gualandi[a], Erika Scavetta[a], Arianna Rivalta[a], Elisabetta Venuti[a], Meganne Christian[b], Vittorio Morandi[b], Angelo Mullaliu[a], Marco Giorgetti[a]*, Domenica Tonelli[a]*

Received 00th January 20xx,
Accepted 00th January 20xx

DOI: 10.1039/x0xx00000x

www.rsc.org/

A novel and enhanced electrosynthesis protocol that allows the deposition of thin films of Co/Al and Co/Fe layered double hydroxides (LDHs) on different supports is hereby proposed. The approach is based on a potentiodynamic cathodic reduction. All the films have been characterised by CVs, powder X-ray diffraction, scanning electron microscopy, and Raman and atomic emission spectroscopies. Moreover, the LDHs electrosynthesised on carbonaceous materials have been also investigated by X-ray absorption spectroscopy to analyse their local metal structure. These substrates are particularly interesting for the plethora of LDHs applications ranging from energy storage, sensing, electrocatalysis, also of industrial importance, due to their low cost, ecocompatibility, and easy handling. In particular, the material was exploited for the 5-(hydroxymethyl)furfural (HMF) electro-oxidation.

Introduction

Layered double hydroxides (LDHs) are lamellar compounds with chemical formula $[M(II)_{1-x}M(III)_x(OH)_2]^{x+}(A_n^{x/n-}) \times mH_2O$, where M(II) and M(III) are metal cations and A^{n-} is the interlayer anion. [1] The LDH properties can be adapted by changing their chemical composition: a wide range of metal cations can be used as M(II) (Mg^{2+}, Ni^{2+}, Co^{2+}, Cu^{2+}, Mn^{2+} or Zn^{2+}) and M(III) (Al^{3+}, Fe^{3+}, Cr^{3+} or Ga^{3+}), and different anions can be intercalated in the interlayers to control the distance between the brucite sheets. [2] Recently, these compounds have been found to be extraordinary materials for electrochemical technologies, for instance in the field of energy storage devices [3-5], as electrode coatings for amperometric or potentiometric sensors [6-8] and as catalysts for water splitting reactions. [9-11]

In order to modify electrode surfaces with LDH films, different methods have been proposed; the most common one consists on synthesizing the LDH through a co-precipitation method and then depositing a fixed amount of a colloidal solution onto the support by drop casting. A drawback of this method is the poor adhesion of the film to the support material.[12] An alternative, cheap and fast route was proposed by Scavetta et al. [13,14] in 2004 consisting in the electrosynthesis of LDH thin films through a potentiostatic reduction of nitrates which leads to hydroxide ions generation. The great advantage of the proposed method is the short time for the electrode fabrication, the well-adhered coatings,[15] even if the signal was not always reproducible. More recently, Tonelli's group[16] has demonstrated that a potentiodynamic approach for synthesising Ni-based LDHs is the most satisfying in terms of reproducibility if compared with the potentiostatic, and galvanostatic methods.

In this work, a study aimed at proposing a novel and alternative potentiodynamic electrosynthesis of Co/Al-NO_3 and Co/Fe-NO_3 LDH is reported.

The electrodeposition of thin films with a Co(II)/M(III) molar ratio of 3:1, which reflects the electrolytic bath composition, is described. Moreover, to verify the versatility of the proposed synthetic protocol, the synthesis has been carried out with two different supports, platinum and Grafoil (a graphitic-like material). Platinum supports have been chosen as reference for the deposition, since Pt was the noble metal previously used to study the electrodeposition mechanism.[17] Grafoil, instead, was chosen since it can be considered a more versatile substrate to be used in a wide range of applications: it is low cost, flexible and environmentally-friendly; these features make Grafoil an optimal candidate for catalytic applications. The films obtained on the electrodes were characterised by cyclic voltammetry (CV), microwave plasma atomic emission spectroscopy (MP-AES), Powder X-ray diffraction (PXRD), Raman spectroscopy, scanning electron microscopy (SEM) and X-ray absorption spectroscopy (XAS).

Finally, among all the possible applications above mentioned, these modified electrodes were tested for the 5-(hydroxymethyl)furfural (HMF) electro-oxidation. Nowadays, HMF molecule is considered a fundamental platform chemical [18], i.e., it is a key precursor for a great number of chemicals which find application in fuel and polymer industry.[19,20]

[a] Dipartimento di Chimica Industriale 'Toso Montanari', Università di Bologna, Viale Risorgimento 4, 40136 Bologna, Italy
[b] Istituto per la microelettronica e i microsistemi (IMM), Consiglio nazionale delle ricerche, Via Gobetti 101, 40129 Bologna, Italy

Electronic Supplementary Information (ESI) available: [details of any supplementary information available should be included here]. See DOI: 10.1039/x0xx00000x

View Article Online
DOI: 10.1039/C8TA12452D

Experimental

Chemicals

Cobalt (II) nitrate hexahydrate (98% pure), aluminium nitrate nonahydrate (>96% pure), 5-hydroxymethyl-2-furaldehyde (99% pure) and sodium hydroxide (98% pure) were supplied by Sigma-Aldrich. Iron (III) nitrate nonahydrate (99% pure) was purchased from Riedel-de Haën. The supporting electrolyte for all the electrochemical experiments was NaOH at the concentration of 0.1 mol/L. The salt solutions were prepared with doubly distilled water. Graphite GTJ (Graphite>99.8%) was used as support and purchased from VED (https://www.ved.it); the geometrical area was 2cm^2, the bulk density was 1.12 g/mL, the resistivity $7.33 \cdot 10^{-4}$ Ω cm; carbon content was established at 99.5%, while ash content at 0.5%. SEM images of this support are reported in SI1. Platinum foil had a geometrical area of 1 cm^2.

Support modification

Cleaning the electrode is a critical step to achieve a well adherent coating. For the graphitic electrode (Grafoil), the surface was rinsed in ethanol for 10 min and then dried to constant weight. The LDH films were deposited on the electrode surface by cathodic reduction of a freshly prepared 0.03 M solution containing M(II) and M(III) at a molar ratio of 3:1. For Al-containing LDHs, the electrochemical reaction was carried out by applying a variable potential (2 CVs cycles between -1.3 and 0.0 V, *vs* SCE) with a scan rate of 30 mV s^{-1}, for Fe containing LDHs the scan rate was 40 mV s^{-1} and the potential window was -1.1 and 0.0V, *vs* SCE. After performing the modification, the electrode was immediately rinsed with water.

For the Pt electrodes, the surface was first polished to a mirror-like surface by a mechanical cleaning, using sand-paper, and then the electrode was submitted to an electrochemical treatment: 250 cycles between -0.25 V and +1.30 V were performed in 0.1 M H_2SO_4 at a scan rate of 1 V s^{-1}. [21] The film was deposited following the same procedure described above but for Al-containing LDHs the scan rate was 20 mV s^{-1}, and for Fe containing LDHs the scan rate was 30 mV s^{-1}.

Apparatus

All the electrochemical tests were carried out in a single compartment, three-electrode cell. Electrode potentials were measured with respect to an aqueous saturated calomel electrode (SCE). A Pt wire was used as the counter electrode. The CV curves were recorded using a CHInstruments Mod. 660C, controlled by a personal computer via CHInstruments software.

X-ray diffraction patterns were obtained with CuKα radiation in reflection mode by means of an X'Pert PANalytical diffractometer equipped with a fast X' Celerator detector. The samples were analysed directly inserting the Pt electrode in the optical centre of the diffractometer. X-Ray Diffraction measurements of LDHs materials on graphite foil were recorded at the MCX beamline at Sincrotrone ELETTRA, Basovizza, Trieste Italy, by using a monochromatic X-ray beam with a wavelength of $\lambda = 0{,}827$ Å. Data were collected in a flat plate configuration by keeping fixed the incident angle at two degrees. The XRD pattern was collected consecutively in the range $5° < 2\theta < 50°$, with steps of 0.02° and an acquisition time of 0.2 s per step.

The morphology and chemical compositions of the LDH films were investigated by Field Emission-Scanning Electron Microscopy (FE-SEM) using a LEO 1530 ZEISS instrument equipped with Schottky emitter, operated at an acceleration voltage variable from 5 to 15 kV, and an Everharte-Thornley and an In-lens detectors for secondary electrons imaging. Energy Dispersive X-ray Spectroscopy (EDS) measurements were performed with an Oxford 30 mm^2 EDS Silicon Drift Detector.

The elemental analysis was performed using an Atomic Emission Spectrometer MP-AES Agilent 4210 controlled by a computer via Agilent MP Expert software.

Raman spectra were recorded with the Renishaw System RM1000. The spectrometer was coupled to a Leica DMLM microscope equipped with 50x, 20x and 5x objectives which allowed, with the 50x objective, a nominal spatial resolution < 2 μm in xy and 4 μm in z. The excitation wavelength was from an argon laser tuned at 514.5 nm. The output power of the laser was around 25 mW, but when needed the light intensity impinging on the film was reduced by neutral density filters to avoid sample damage.

Samples for the XAS measurements were prepared following the procedure described above with the unique exception of the scan rate, which was 10 mV s^{-1}. XAS experiments were performed at ELETTRA Synchrotron Radiation Laboratory (Basovizza, Trieste), on the XAFS beam line 11.1 [22], recording the data in fluorescence mode using a large area Si drift diode detector (KETEK). XAS spectra were recorded at the Co and Fe K-edge (7709 eV and 7112 eV, respectively) using a Si(111) double crystal monochromator. Extended X-Ray Absorption Fine Structure (EXAFS) curves were recorded at room temperature. X-Ray Absorption Spectroscopy spectra were deglitched, calibrated, and normalized using the Athena program.[23] The pre-edge background was removed by subtraction of a linear function extrapolated from the pre-edge region, and the XANES spectra were normalized at the unity by extrapolation of the atomic background. The EXAFS analysis was performed by using the GNXAS package[24] that considers Multiple Scattering (MS) theory. Briefly, the method is based on the decomposition of the EXAFS signals into a sum of several Single scattering (SS) and Multiple Scattering (MS) contributions, *i.e.*: the n-body terms. It allows the direct comparison of the raw experimental data with a model theoretical signal. The procedure avoids any filtering of the data and allows a statistical analysis of the results. The theoretical signal is calculated ab-initio following a previously published structural model for LDHs [25] that has been adapted to this set of samples and contains the relevant two-body γ(2), three-body γ(3) and four body [26] γ(4) MS terms. For the case of the Co-edge the following n-body terms have been included in the fitting procedures: the two-atom contributions γ(2) Co-O with degeneracy of six and the two-atom contributions γ(2) Co--Co with degeneracy of six. This also accounts for two Co--Fe interactions at the same distance. This approximation holds due

View Article Online
DOI: 10.1039/C8TA11812D

to the relative identical scattering power of both metals. Also, the following n-body terms have been included in the fitting procedures for the Fe K-edge case: the two-atom contributions $\gamma(2)$ Fe-O with degeneracy of six and the two-atom contributions $\gamma(2)$ Fe--Co(Fe) with degeneracy of six. Data analysis was performed by minimising a $\chi 2$-like residual function that compares the theoretical signal, αmod(E), to the experimental one, αexp(E). The phase shifts for the photoabsorber and backscattered atoms were calculated ab-initio according to the muffin-tin approximation and allowing 5-15% overlap between the muffin-tin spheres. The Hedin-Lundqvist complex potential[27] was used for the exchange-correlation potential of the excited state. The core hole lifetime[28] was fixed to the tabulated value and included in the phase shift calculation. The experimental resolution in the fitting analysis was about 1 eV, in agreement with the stated value for the beamline used.

To analyse the products of the oxidation procedure, the residue obtained after evaporation of the solvent was taken from the cell and suspended in 2 mL 0.1M NaOH. 50 µL of this solution were diluted to 5 mL and analysed by means of an Agilent Infinity 1200 liquid chromatograph equipped with an Aminex HPX 87-H 300 mm 7.8 mm column, using a 0.005 M H_2SO_4 solution as the mobile phase. The identification of the products was achieved using reference commercial compounds and their concentrations were determined from the calibration curves (correlation coefficient = 0.999). The HMF conversion (%) and the selectivity for the oxidation products were calculated using the following equations:

$$\text{HMF conversion}(\%) = \frac{\text{mol of HMF consumed}}{\text{mol of initial HMF}} \text{x } 100$$

$$\text{Selectivity}(\%) = \frac{\text{mol of product}}{\text{mol of HMF converted}} x100$$

The Faradaic efficiency (FE) of FDCA product was calculated by

$$\text{FE } (\%) = \frac{\text{mol of FDCA formed}}{\text{mol of total electrons passed}/6} \text{x } 100$$

Moreover, ^{1}H-NMR spectra were recorded at 400 MHz, on a Bruker Avance 400 spectrometer.

Results and discussion

Electrochemical deposition on Platinum and Grafoil

In order to find the best experimental conditions to obtain an LDH film, the electro-synthesis was carried out both on Pt foil and on carbonaceous materials, investigating some parameters such as the scan rate and the potential window. Recently, our group has proposed a potentiodynamic approach[16] for the electrochemical reduction of a nitrates solution of nickel and aluminium which consists of several reactions that contribute to the precipitation, close and on the electrode surface, of the LDH. However, the precipitation of single metal hydroxides or oxides could be a side reaction. The reactions, causing the disappearance of H^+ ions and/or the generation of OH^- ions, induce a pH increase necessary for the LDH precipitation, and they are as follows [17,29,30]:

$H^+ + e^- \rightarrow H_{ads}$

$2H^+ + 2e^- \rightarrow H_2$ $\quad E°=0.0V$

$NO_3^- + 2H^+ + 2e^- \rightarrow NO_2^- + H_2O$ $\quad E°=0.93V$

$NO_3^- + 10H^+ + 8e^- \rightarrow NH^{4+} + 3H_2O$ $\quad E°=0.36V$

$2H_2O + 2e^- \rightarrow H_2 + 2OH^-$ $\quad E°=-0.83V$

$NO_3^- + H_2O + 2e^- \rightarrow NO_2^- + 2OH^-$ $\quad E°=0.01V$

The mechanism of LDH electrodeposition has been proposed to possibly occur in two different ways: the first one involves the precipitation of $Al(OH)_3$ followed by the insertion of the bivalent cation to form the clay structure. The second proposed mechanism is the direct precipitation of the LDH without involving the hydroxide of the trivalent metal[14]. It is worth mentioning that various chemical synthesis approaches have been described in the literature and there is not a unique explanation for the reactions sequence of the LDH production, even for the chemical route.[31] It is also important to notice that the support characteristics (i.e., morphology, composition, and electrical conductivity) determine its activity in terms of reduction potential at which the above reported reactions occur, current distribution and mass transfer processes. In fact, it is well known that the electrochemical reduction of nitrate is a complex process, that depends on a lot of factors (such as the support, but also temperature, pH and composition of the bath, etc.)[32]. Moreover, during the electrodeposition of LDH compounds, two further issues must be considered: the first one is the growing of the film, which alters the conductivity and the area available for nitrate adsorption; the second one is related to the continuous modification of pH and, therefore, of nitrate reduction potential and electrochemical products.[29]

The cyclic voltammetric curves recorded during the synthesis of the Co/Al-NO_3 and Co/Fe-NO_3 LDHs using the newly proposed synthetic path are displayed in Figure 1.

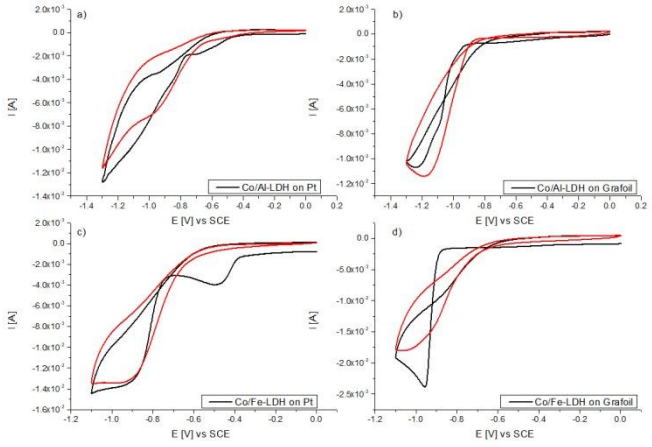

Figure 1. CV curves recorded at Pt (a and c) and Grafoil (b and d) substrates soaked in solutions of Co and Al (a and b) and Co and Fe nitrates (c and d)

From the CVs, it is possible to note a small difference between the two supports as to the first voltammetric cycle (displayed in

black): in the case of platinum two peaks are detectable (the less cathodic one can be ascribable to hydrogen evolution, the other to nitrate reduction), whereas for Grafoil just one peak can be seen.

For Co/Al-NO_3 the two peaks are located for Pt at -0.6 and -1 V, whereas for Grafoil the peak is at -1.1V. For Co/Fe-NO_3 a shift toward less cathodic potentials is registered: the two peaks on Pt are at -0.4 and -0.9 V, respectively, whereas on Grafoil the peak is at -0.97 V.

Another difference can be observed in the total charge passed during the deposition, which is practically the same for both electrodes. Considering that the geometrical area of Pt foil is half that of the Grafoil, it means that when Pt is used as a support the charge is double. This can be explained by a higher efficiency of LDHs formation on Pt compared to Grafoil.

Physical characterisation of the synthesised LDHs

With the aim to verify the structure of the LDHs, PXRD analysis was carried out directly on the graphitic and Pt electrodes.

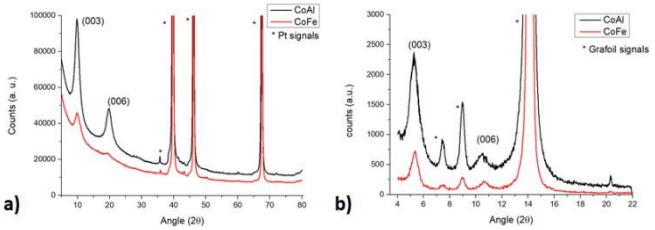

Figure 2. PXRD patterns of the LDHs electro-synthesised on a) Pt and b) Grafoil. The clipped reflections are due to Pt or Grafoil.

As can be seen from Figure 2, the patterns of all the samples show the main diffraction maxima typical of the LDH phase, indexed as 003 and 006 reflections.

As far as the Co/Al-LDH is concerned it is evident that this material displays the narrowest reflections when synthesised on Pt, its crystal domains must be larger and better formed compared to the other LDHs.

Generally, it is possible to confirm that the substrate plays a central role in the formation of the crystal domains: in fact, on Pt it was possible to collect the pattern with a conventional X-ray tube using the Cu Kα radiation ($\lambda = 1.5406$ Å). On the other hand, with Grafoil as a support, the same instrument does not allow us to gather a clear signal for LDH phase. The XRD pattern was successfully recorded using a synchrotron radiation source ($\lambda = 0.827$ Å). Comparing the results obtained for the two supports, it should be noticed that on Pt the reflections are generally narrower than on Grafoil, suggesting a better formation of the crystalline phase.

Eventually, for both Pt and Grafoil, it is remarkable to notice that the new approach for the electrosynthesis permits a direct access to the analytical characterisation of LDHs. Unlike, by using the potentiostatic method previously reported [7], a good signal was recorded only after 10 repetitions of the synthetic protocol.

Morphological characterisation of the synthesised LDHs

View Article Online
DOI: 10.1039/C8TA11812D

The morphological characterisation of the LDHs electro-synthesised on Grafoil and Pt was performed using FE-SEM. All the supports appeared homogeneously covered and no detachment of the film was observed in any case. Investigating more thoroughly the LDHs films, different compactness and thicknesses of the coatings were discerned. Figure 3 illustrates the morphologies of the materials on Pt and Grafoil.

The images show great differences among LDHs and supports. When Grafoil (Fig. 3 c, d, g, h) was used for the electrodeposition, all the LDH coatings appeared very compact and consisted of basically round particles with a uniform size distribution. In particular, the smallest particles (10-20 nm) were observed for the Fe-containing LDH. Furthermore, the film is so compact that the particles seem almost fused to each other. This observation can be further confirmed from Figure 3d, which shows a cross-section: the material seems to display a flower-like morphology on the layer in contact with the substrate whereas in the upper part it looks more compact. In the case of Pt, the morphology of the LDH coatings shows surprising differences (Fig. 3 a, b, e, f). As far as the Co/Al LDH is concerned the particles appear in spherical groups on which flower-like architectures are grown, indicating the formation of 3D hierarchical nanostructures. In case of the Co/Fe LDH the morphology consists of well-defined highly interconnected tubular particles which are the largest (about 1 μm long and 150 nm wide) among the electro-synthesised LDHs. At the best of our knowledge, this kind of structure has never been reported for an electrochemical synthesis route of Co/Fe and Co/Al-LDHs. In both cases, underneath the larger particles there was a more compact film similar to that observed on Grafoil.

A qualitative evaluation of the adhesion between thin coatings and substrates can be made using a scratch testing technique. In this work, the test was performed applying a constant load (0.1N) on the LDH coating by a Rockwell C diamond indenter while the specimen moved horizontally. The SEM images obtained for the LDH films on Pt and Grafoil surfaces with scratch tracks are reported in SI2 (a, b, c, d), respectively. In the first case, the failure is only confined into the scratch track (transverse cracking) and the coating resulted well-adherent, as already reported for the films obtained from potentiostatic procedure.[15] The Grafoil support, due to its intrinsic morphology, is particularly fragile and, using the indenter, the flakes of Grafoil tend to detach one to another and fold up (SI2b). Consequently, when thin LDH films are electro-deposited on Grafoil and the adhesion is good, they follow the shape of the support track produced by the indenter, as expected and pointed out from Figures SI2c and d (images after the scratch test at 2 magnifications).

Moreover, the films deposited on Pt are thicker than those obtained on the graphitic substrate (≈3 μm compared to 800 nm). The LDH films were also characterised by semi-quantitative SEM/EDS analysis to determine the M(II)/M(III) atomic ratio (see SI3). All the values were around 3, practically identical to the molar ratio of the cations present in the electrolytic solutions used for the synthesis. Moreover, in order

View Article Online
DOI: 10.1039/C8TA11813D

to validate the SEM/EDS values, MP-AES was also performed. The average results of three independent measurements for Co/Al and Co/Fe-LDHs was 3.3 and 3.2, respectively. These values confirm the SEM/EDS analysis and are compatible with an LDH stoichiometry.

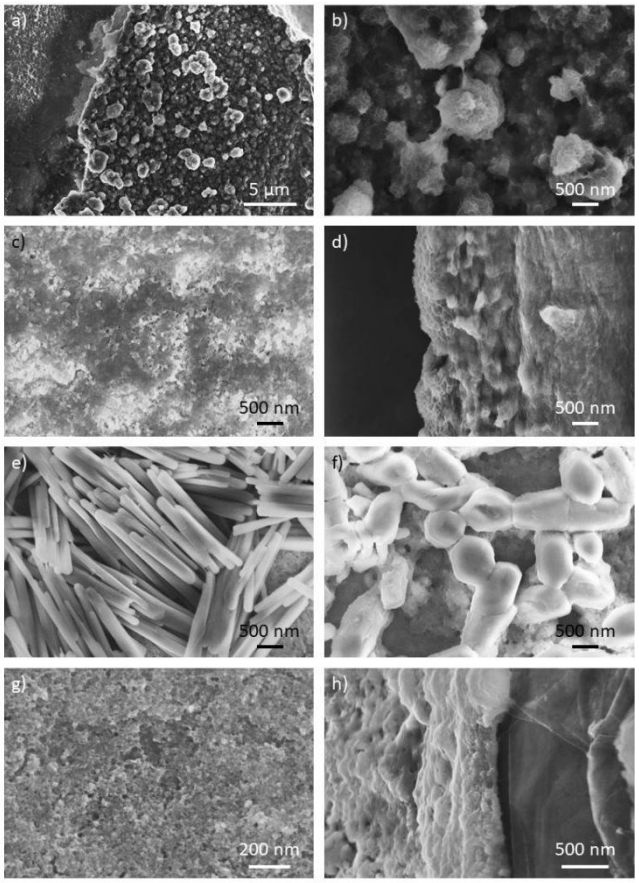

Figure 3. SEM images of thin films of Co/Al-LDH deposited on a) and b) Pt, c) and d) Grafoil; and of Co/Fe-LDH deposited on e) and f) Pt, g) and h) Grafoil.

Raman spectroscopy

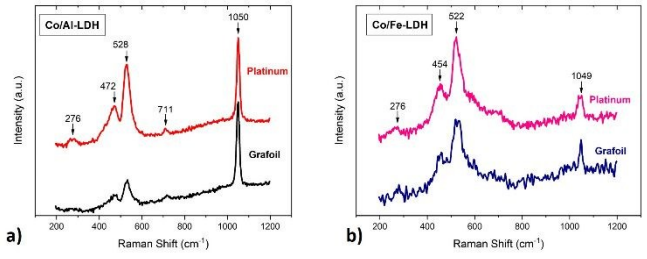

Figure 4. Raman spectra of left) Co/Al-LDH on Pt and Grafoil and right) Co/Fe-LDH on Pt and Grafoil

The Raman spectra of the Co/Al and Co/Fe-LDHs in the wavenumber region 200-1200 cm^{-1}, which is diagnostic for these LDHs, are reported in Figure 4. The main spectral features of the Co/Al LDHs are the broad Raman shift at 472 cm^{-1}, with a shoulder at lower wavenumbers, and the sharper bands at 528 and 1050 cm^{-1}. Much weaker features appear below 300 cm^{-1} (which should be ascribed to lattice modes) and at 711 cm^{-1}. A thorough discussion of the Raman spectrum is not of interest here, and the analysis of the bands at 472 and 528 cm^{-1}, typical of these materials, must rely on previous studies on the vibrational properties of cobalt hydroxides and cobalt–based LDHs. [10,33-35]

In the literature there is no general agreement about the assignment, but it is reasonable to assume that the band at 528 cm^{-1} is correlated to the strong band observed at 522 cm^{-1} in $Co(OH)_2$, and, therefore, is assigned to hydroxyl groups bound to the Co cation, despite the small mismatch with the data for chemically synthesised Co/Al-LDHs. The broader feature at 472 cm^{-1} appears to correspond to the 471 cm^{-1} band observed in the IR spectrum of a Co/Al hydrotalcite-like compound [33], and assigned to hydroxyl groups bound to Al. The occurrence of a band at 454 cm^{-1} in Co/Fe-LDH Raman spectrum (vide infra) has suggested[10] that the shoulder of this band again arises from the hydroxyl bound to Co cation. Finally, also the strong band at 1050 cm^{-1} lies at lower wavenumbers and with much larger intensity than reported in Ref.[10], where the weak feature observed at 1057 cm^{-1} in Co/Al-LDH is virtually absent in Co/Fe-LDH. In this work, the band is assigned to OH deformation modes, based on previous observations, but an alternative assignment, relying on the high intensity, could be the symmetric stretching of the nitrate anion.

Similar to the Co/Al-LDHs, the Co/Fe samples show bands at shifts of 454 and 521 cm^{-1} (Figure 4 right). It should be noted that the band at 1049 cm^{-1} is barely detected in any of the Co/Fe LDH samples, in agreement with the literature data.

Generally, the Raman spectra of the Co/Al-LDHs display a stronger intensity with respect to those of Co/Fe-LDHs, regardless of the support. Although a quantitative estimate is not possible, such a behaviour is unlikely to be related to an intrinsic property of the compound, but it is usually related to a higher degree of crystallinity of the Co/Al system.

Most importantly, and independently of the details of the spectral analysis, the Raman measurements have been employed to probe the chemical identity of the materials obtained on the two different electrodes used for the growth. The spectra of LDHs sharing the same cations on Pt and Grafoil are virtually identical and, therefore, we can assume that the structure and the composition of the LDH do not depend on the nature of the support.

X-ray Absorption Spectroscopy (XAS)

Due to its strong sensitivity for the metal site, local structural and electronic information can be gained by looking at the X-Ray Absorption spectra of the electrodeposited materials at both Fe and Co sites in the LDHs. Since we are interested in bulk characterisation of the electrodeposited LDHs, XAS measurements were recorded in transmission mode and, therefore, only the graphitic substrate has been considered for this set of data (the Pt substrate would absorb a large fraction of the X-ray beam). In addition, Grafoil can be considered a

View Article Online
DOI: 10.1039/C9TA12125

more versatile substrate to be used in a wide range of applications, and it is cheap and eco-friendly.

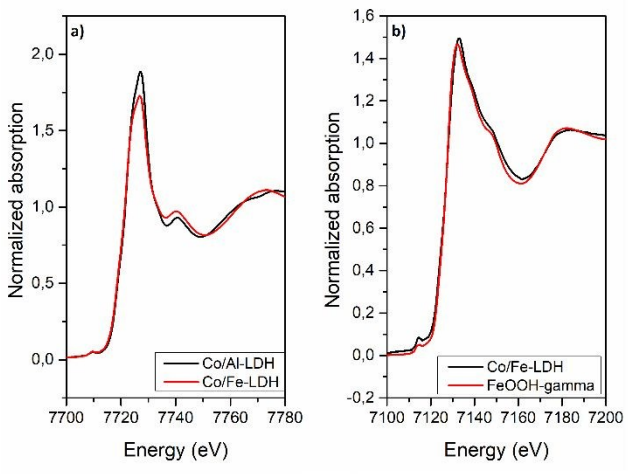

Figure 5. Comparison of the XANES spectra recorded for Co/Fe and Co/Al-LDH at Co K-edge (a) and comparison of Co/Fe-LDH with FeOOH at the Fe K edge (b).

Fig. 5a shows the comparison of the XANES spectra at Co K-edge recorded for both Co/Fe and Co/Al LDHs. Both traces are almost superimposable, and, therefore, the local structure and charge associated to the Co site appear identical in the two electrodeposited LDHs. How much that charge is? This can be evaluated by looking at both pre-edge peak position and overall shape of previously published Co(II) XANES data,[36] which indicated a Co(II) formal oxidation state of an atom in an octahedral environment.

Fig. 5b displays the XANES at the Fe K-edge of the Co/Fe LDH. The curve is characterised by a pre-edge peak at about 7114 eV which is related to the 1s-3d electronic transition and can be used as a fingerprint for the local charge around Fe. The position and the intensity of such a peak indicate mainly the occurrence of the Fe(III) oxidation state in an octahedral environment[37]. Confirmation of such an assignment comes from a comparison with a Fe(III)OOH reference sample.

To explore more deeply the local structure around the metals of the deposited LDHs an EXAFS analysis has been performed at both Co and Fe K-edges. Figure 6 displays details of the best fit procedure, for the Co/Fe LDH. Due to the presence of two metals sites, the structure of this electrodeposited material has been analysed from the two photoabsorbers, i.e., Co and Fe. The Fourier Transforms (FTs) of the corresponding EXAFS signals are depicted in the panels (c) and (d). This plot displays the pseudo-radial distribution of the atoms surrounding the central one and suggests that two main peaks contribute majorly to the experimental photo-absorption process at both metal sites. They are related to the typical LDH structure where the first peak is due to the first atomic shell surrounding the Co and the second peak, at about 2.6 Å, is associated with the second coordination shell, formed by 6 metal atoms (4 Co and 2 Fe). The same coordination is observed at the Fe site. Therefore, only these signals have been used in the fitting procedure. This is clearly shown in the panels (a) and (b) of the Figure for both Co and Fe K-edges, respectively. These plots report various theoretical contributions to the total EXAFS signal. The Co-O and Fe-O first shells largely contribute to the total signal in their respective panels but the metal-metal signal in the second shell is rather important for the interpretation of the total experimental one. It is also interesting to notice that the two-body $\gamma(2)$ Fe -- Co signal has a smaller intensity when compared to that of the $\gamma(2)$ Co -- Co one. This can be ascribed to a structural disorder at the Fe site.

Table 1 reports the inter-atomic distances and the corresponding EXAFS Debye-Waller factors (σ^2, best-fit) of the investigated electrodeposited LDHs. The statistical errors associated with the parameters are indicated in parentheses. They were determined by correlation maps (contour plots) for each pair of parameters. These plots were selected among the parameters having a strong correlation to reflect the highest error. The inner elliptical contour corresponds to the 95% confidence level. Panels (e) and (f) report two examples for the highly correlated Co-O and Fe-O variables.

The trivalent metal (Fe or Al) influences the local structure of the electrodeposited LDHs, even at the Co site. The Co-O interaction significantly enhances from 2.053 to 2.082 Å by substituting Fe^{3+} with Al^{3+}, while the interaction at the second shell holds at a value of about 3.11-3.13 Å for both Co--Co and Co--Al (only in the Co/Al-LDH case). Lower EXAFS bond variances are observed in Al-based LDHs as seen from both σ^2 Co-O and σ^2 Co--Co comparison. This suggests a more regular and crystalline structure of the Co/Al with respect to the Co/Fe-LDHs, probably because less strain is induced by the smaller Al atomic size, in good agreement with the better crystallinity pointed out by XRD data.

A comparison of the EXAFS bond variance of the Co/Fe-LDH second shell reveals a large contribution from the structural disorder at the Fe site with respect to the Co one, as previously suggested by the Figure 6 panel (a) and (b). This fact can be extended to other LDHs (e.g. Ni/Fe LDH) where the trivalent site is found to be more structurally disordered than the divalent one.[2]

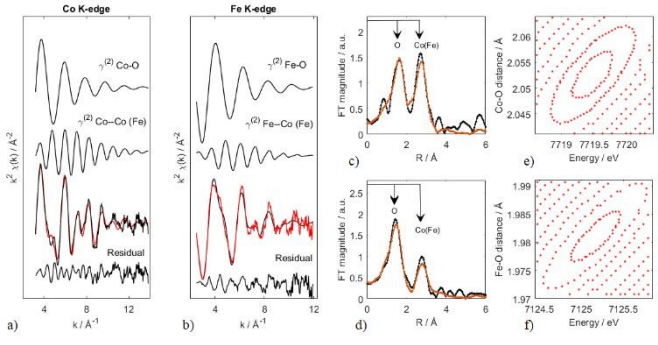

Figure 6. Best fit of Co/Fe LDH at both Fe and Co K-edges. Panels (a) and (b) show the details of the EXAFS analysis for the Co and Fe edge, respectively, in terms of individual EXAFS contributions to the total theoretical signal. The comparison of the total theoretical signal (black curve) with the experimental one (red curve) is also shown. The residual signal is reported at the

bottom. Panels (c) and (d) display the fit of the corresponding FTs of EXAFS. Panels (e) and (f) display the contour plot for the error determination of the Co-O and Fe-O first shell distances.

Table 1. EXAFS Analysis. Atomic first and second shell distances and corresponding EXAFS Debye-Waller factors of the pristine and oxidized LDHs. Errors (in parentheses) were determined by Contour plots (see Fig. 6 e and f).

Parameter	Co-Al/LDH	Co-Fe/LDH	
	Co K-edge	Fe K-edge	Co K-edge
Co-O /Å	2.053(4)		2.082(8)
$\sigma^2_{Co\text{-}O}$ /Å^2	0.008(1)		0.006(1)
$CN_{Co\text{-}O}$	6		6
Co-Co /Å	3.135(6)		3.11(1)
$\sigma^2_{Co\text{-}Co}$ /Å^2	0.010(1)		0.0064
$CN_{Co\text{-}Co}$	6		4
Co-Al /Å			3.11(2)
$\sigma^2_{Co\text{-}Al}$ /Å^2			0.005(2)
$CN_{Co\text{-}Al}$			2
Fe-O /Å		1.981(5)	
$\sigma^2_{Fe\text{-}O}$ /Å^2		0.010(1)	
$CN_{Fe\text{-}O}$		6	
Fe-Co(Fe)/Å		3.116(8)	
$\sigma^2_{Fe\text{-}Co(Fe)}$ /Å^2		0.017(2)	
$CN_{Fe\text{-}Co(Fe)}$		6	
E_0 / eV	7719.4(5)	7125.1(5)	7722.1(8)
S_0^2	0.70(4)	0.71(5)	0.70(3)

Electrochemical LDHs characterisation

The electrochemical characterisations of the LDHs were performed. A preliminary check of the film stability was studied by recording several CV curves for the electro-synthesised LDHs. The signals were superimposable for hundreds of cycles at both supports, and this suggested a good adhesion of the clays. Therefore, the mechanical and electrochemical stability can be considered very good.

The first CV scan recorded for both LDHs was remarkably different from the following ones (Figure 7): as already reported,[13] during this cycle an irreversible reaction occurs involving Co(II) sites.

After stabilization two peak couples can be observed for the Co/Al-LDH on both supports with E_{pa}= 0.14 V and E_{pa}=0.42 V. The feature at around 0.14 V is hardly detectable for Pt, whereas it displays a good intensity in the case of Grafoil.

These peaks are related to Co redox system, according to equation 1 and 2:[13]

1) LDH−Co (II) + OH^-_{sol} ⇆ LDH(OH) – Co (III) + e^-
2) LDH−Co (III) + OH^-_{sol} ⇆ LDH(OH) – Co (IV) + e^-

As can be observed from figures 7 c) and 7 d) the signals of three LDHs coming from independent depositions are superimposable both for Grafoil and Pt supports.

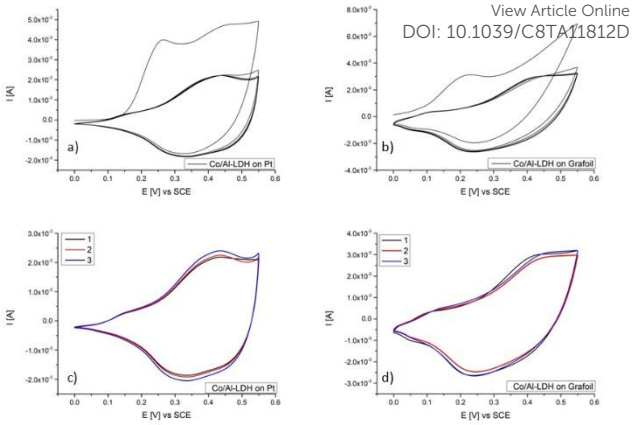

Figure 7. CVs of Co/Al-LDH on a and c) Pt, b and d) Grafoil. Figures c) and d) show the reproducibility of the electrodeposition since they refer to three independent syntheses.

In Figure 8 CVs recorded for the Co/Fe-LDH are shown. In this case only one peaks system is evident on both supports, but its position is dependent on the material used as a substrate. E_{pa} is located at 0.15 V for Pt and 0.20 V for Grafoil.

In this case the reproducibility of the electrosynthesis on Grafoil seems slightly better that on Pt (Figure 8 c and d).

Eventually, the optimal reproducibility observed for the potentiodynamic electrosynthesis of Co/Al and Co/Fe-LDHs on both substrates and, especially, on Grafoil is a striking result for the real LDHs applications. In fact, the graphitic support is cheap and can be used in several fields such as energy storage, sensing, industrial electrocatalysis, etc.

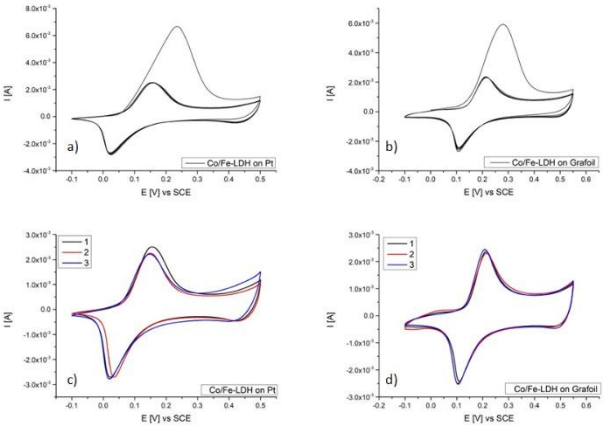

Figure 8. CVs of Co/Fe-LDH on a and c) Pt and b and d) Grafoil. Figures c) and d) show the reproducibility of the electrodeposition since they refer to three independent synthesis.

View Article Online
DOI: 10.1039/C9TA11842D

Electrochemical HMF oxidation

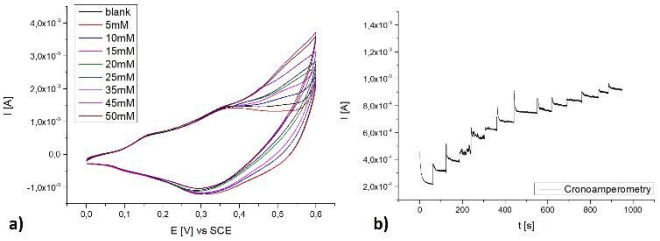

Figure 9. a) CVs recorded at a Co/Al-LDH coated Grafoil in 0.1 M NaOH, containing HMF at different concentrations, ν = 10 mVs^{-1}; b) I *vs* time plot obtained for the same Co/Al-LDH at + 0.5 V in 0.1 M NaOH under magnetic stirring, while the HMF concentration was increased by progressive additions of a concentrated solution

A preliminary study of the oxidation of HMF was carried out by CV. Firstly the suitable experimental working conditions were explored in terms of applied potential. As an example, Fig. 9a shows the CVs recorded at Grafoil coated with Co/Al-LDH following the addition of HMF different amounts to a 0.1 M NaOH solution. An increase of the anodic current is recorded which is proportional to HMF concentration. The chronoamperometric response was obtained by setting the potential at +0.5 V (Fig. 9b). The same experiments were carried out using Pt as the support and all of them were repeated also for the Co/Al-LDH. The sensitivities and the LOD values of the four calibration lines are reported in Table 2. The Co/Al-LDH displays a lightly better performance as to the sensitivity in respect to the Co/Fe-LDH, independently on the support. As expected, the same material displays the same LOD in despite of the support and the values are similar for both LDHs. Moreover, the reproducibility of the sensitivity values for the HMF determination, as expressed by the slopes of the calibration lines, is satisfactory as expected by the good reproducibility of the newly proposed electrodeposition.

Table 2.LOD values and sensitivity obtained from the calibration lines for HMF determination by chronoamperometry

	Sensitivity ($AM^{-1}cm^{-2}$)	**LOD (M)**
Co/Al-LDH on Pt	0.417 ± 0.008	$1.69*10^{-4}$
Co/Al-LDH on Grafoil	0.394 ± 0.006	$1.73*10^{-4}$
Co/Fe-LDH on Pt	0.070 ± 0.002	$2.23*10^{-4}$
Co/Fe-LDH on Grafoil	0.069 ± 0.004	$2.12*10^{-4}$

As a proof of concept, Co/Al-LDH on Grafoil has also been tested for an exhaustive electrolysis (E = +0.5 V, t = 72 h, nitrogen atmosphere). Nowadays, research efforts are devoted in developing processes for production of 2,5-furandicarboxylic acid (FDCA) to be employed as a monomer in industrial synthesis. In this scenario, the proposed system results in a complete noble metal-free catalyst. Moreover, the support must also be considered in a process development, since a catalyst prepared with the same metal active phase might display different catalytic performances depending on the support used. Thus, in this wide range of studies on innovative processes aiming at the preparation of metal-supported catalysts, it is here proposed Grafoil as support since it is low cost, environmentally friendly, and easy to handle, as already mentioned.

The solution coming from the exhaustive electrolysis was analysed by HPLC equipped with diode array detector (see SI 4) and ^{1}H-NMR (see SI 5-6) in order to identify the oxidation products.

Neither HPLC nor ^{1}H-NMR shows presence of HMF, confirming a virtual conversion of 100%. 5-Hydroxymethyl-2-furancarboxylic acid (HMFCA) and FDCA are formed as major products, and an unidentified aliphatic product can be also detected. This product was investigated also with ESI-MS spectrometry (see SI 7), giving a molecular weight of 242.

The selectivity toward FDCA, calculated from HPLC, results 49%, while toward HMFCA is 37%. The Faradaic efficiency was calculated to be 40.8%. When analysing the FE, it must be noticed that the oxygen evolution reaction competes with the electrocatalytic oxidation of HMF to FDCA in alkaline media, probably causing a decrease of the selectivity. Summarising, the above reported results suggest that the proposed chemically modified electrodes can be considered an interesting approach to produce FDCA from HMF catalytic oxidation.

Conclusions

Films of Co/Al and Co/Fe-LDHs were prepared by a novel and better performing electrodeposition route. Both Pt and carbon-based materials were investigated as supports. All the characterisations confirm the LDH structure of the electro-synthesised materials.

PXRD suggests better-formed crystal domains with respect to the previously proposed potentiostatic approach. Another remarkable result is related to the morphology of the Co-containing LDHs on Pt, which display a well-defined nanostructure.

The best films in terms of stability and reproducibility have been obtained on carbon-based materials, whereas a greater charge has been recorded on Pt, which also means a larger amount of deposited material.

Finally, the modified electrodes were employed for the electro-oxidation of HMF, displaying good performances, so suggesting the importance of a further investigation for applications in the field of industrial catalysis.

In conclusion, we propose a robust and highly reproducible electrosynthesis procedure that can be applied to different supports and this represents on outstanding opportunity in view of the large number of LDHs applications.

View Article Online
DOI: 10.1039/C8TA11812D

Conflicts of interest

There are no conflicts to declare.

Acknowledgements

Authors are grateful to the University of Bologna, Italy, for providing financial support. XAS experiments at ELETTRA Sincrotrone Trieste were partially supported by the proposal Ceric 20172042 (MG as PI). Thanks are also due to Dr. M. Gazzano for performing PXRD measurements. Moreover, thanks need to be done to Dr. Jasper R. Plaisier for performing XRD and Giuliana Aquilanti for XAS at ELETTRA. Authors are also grateful to Daniel Pecorari and Michele Mancinelli for performing 1H-NMR experiment and to Danilo Bonincontro for performing HPLC separation. The authors acknowledge also professor Casagrande for performing ed evaluating scratch tests. The European Union's Horizon 2020 Research and Innovation Programme (Grant Agreement no. 696656 Graphene Flagship) for funding. This research was also funded by the Italian Ministry of Research (MIUR) within PRIN-2015 Project No. NEWLI2015CL3APH.

References

1 K. H. Goh, T. T. Lim and Z. Dong, *Water Res.*, 2008, **42**, 1343–1368.
2 G. B. B. Varadwaj and V. O. Nyamori, *Nano Res.*, 2016, **9**, 3598–3621.
3 Y. Vlamidis, E. Scavetta, M. Giorgetti, N. Sangiorgi and D. Tonelli, *Appl. Clay Sci.*, 2017, **143**, 151–158.
4 H. Chen, L. Hu, M. Chen, Y. Yan and L. Wu, *Adv. Funct. Mater.*, 2014, **24**, 934–942.
5 S. Yao, P. Li, L. Wang, G. Chen and Y. Jiao, *New J. Chem.*, 2019, 3139–3145.
6 I. Gualandi, E. Scavetta, Y. Vlamidis, A. Casagrande and D. Tonelli, *Electrochim. Acta*, 2015, **173**, 67–75.
7 E. Scavetta, L. Guadagnini, A. Mignani and D. Tonelli, *Electroanalysis*, 2008, **20**, 2199–2204.
8 X. Xu, X. Zou, S. Wu, L. Wang, X. Niu, X. Li, J. Pan, H. Zhao and M. Lan, *Anal. Chim. Acta*, 2019, **1053**, 89–97.
9 Y. Vlamidis, E. Scavetta, M. Gazzano and D. Tonelli, *Electrochim. Acta*, 2016, **188**, 653–660.
10 F. Yang, K. Sliozberg, I. Sinev, H. Antoni, A. Bähr, K. Ollegott, W. Xia, J. Masa, W. Grünert, B. R. Cuenya, W. Schuhmann and M. Muhler, *ChemSusChem*, 2017, **10**, 156–165.
11 J. Guo, X. Yang, S. Bai, X. Xiang, R. Luo, J. He and A. Chen, *J. Colloid Interface Sci.*, 2019, **540**, 9–19.
12 S. Miyata, *Clays Clay Miner.*, 1983, **31**, 305–311.
13 E. Scavetta, B. Ballarin, M.Gazzano and D. Tonelli, *Electrochim. Acta*, 2009, **54**, 1027–1033.
14 E. Scavetta, A. Mignani, D. Prandstraller and D. Tonelli, *Chem. Mater.*, 2007, **19**, 4523–4529.
15 E. Scavetta, A. Casagrande, I. Gualandi and D. Tonelli, *J. Electroanal. Chem.*, 2014, **722–723**, 15–22.
16 I. Gualandi, Y. Vlamidis, L. Mazzei, E. Musella, M. Giorgetti, M. Christian, V. Morandi, E. Scavetta and D. Tonelli, *ACS Appl. Nano Mater.*, 2019, **2**, 143–155.
17 E. Scavetta, I. Gualandi, D. Tonelli, C. Mousty, V. Prevot and M. Monti, *Electrochim. Acta*, 2014, **152**, 75–83.
18 C. Megías-Sayago, A. Lolli, S. Ivanova, S. Albonetti, F. Cavani and J. A. Odriozola, *Catal. Today*, 2018, 0–1.
19 J. N. Chheda, Y. Román-Leshkov and J. A. Dumesic, *Green Chem.*, 2007, **9**, 342–350.
20 A. Gandini, *Green Chem.*, 2011, **13**, 1061–1083.
21 I. Gualandi, A. G. Solito, E. Scavetta and D. Tonelli, *Electroanalysis*, 2012, **24**, 857–864.
22 G. Aquilanti, M. Giorgetti, R. Dominko, L. Stievano, I. Arčon, N. Novello and L. Olivi, *J. Phys. D. Appl. Phys.*, 2017, **50**, 1–12.
23 B. Ravel and M. Newville, *J. Synchrotron Radiat.*, 2005, **12**, 537–541.
24 A. Filipponi and A. Di Cicco, *Phys. Rev. B*, 1995, **52**, 15135–15149.
25 Y. Vlamidis, S. Fiorilli, M. Giorgetti, I. Gualandi, E. Scavetta and D. Tonelli, *RSC Adv.*, 2016, **6**, 110976–110985.
26 M. Giorgetti, M. Berrettoni, A. Filipponi, P. J. Kulesza and R. Marassi, 1997, 108–112.
27 L. Hedin and B. I. Lundqvist, *J. Phys. C Solid State Phys.*, 1971, **4**, 2064–2083.
28 M. O. Krause and J. H. Oliver, *J. Chem. Phys. Ref. Data*, 1979, **8**, 329–337.
29 E. Bernardi, M. Monti, D. Tonelli, P. H. Ho, P. Benito, A. Vaccari, L. Nobili, G. Fornasari and E. Scavetta, *Electrochim. Acta*, 2016, **222**, 1335–1344.
30 E. Scavetta, B. Ballarin, M. Giorgetti, I. Carpani, F. Cogo and D. Tonelli, *J. New Mater. Electrochem. Syst.*, 2004, **7**, 43–50.
31 A. V. Radha and P. V. Kamath, *Bull. Mater. Sci.*, 2003, **26**, 661–666.
32 C. Milhano and D. Pletcher, in *Modern Aspects of Electrochemistry*, 2009, pp. 1–61.
33 J. Pérez-Ramírez, G. Mul, F. Kapteijn and J. A. Moulijn, *J. Mater. Chem.*, 2001, **11**, 821–830.
34 R. L. Frost, J. Yang, H. Liu, W. N. Martens and R. L. Frost, 2009, 111–119.
35 J. T. Kloprogge, D. Wharton, L. Hickey and R. L. Frost, *Am. Mineral.*, 2002, **87**, 623–629.
36 D. Totir, Y. Mo, S. Kim, M. R. Antonio and D. A. Scherson, *J. Electrochem. Soc.*, 2000, **147**, 4594.
37 A. Mullaliu, G. Aquilanti, P. Conti, J. R. Plaisier, M. Fehse, L. Stievano and M. Giorgetti, *J. Phys. Chem. C*, 2018, **122**, 15868–15877.